Shock Tubes and Shock Tunnels: Design and Experiments

Raymond Brun
Université d'Aix-Marseille, France

brun-raymond@orange.fr

1.0 INTRODUCTION

The experimental study of non-equilibrium gas flows requires the design, creation and operation of specific facilities and the development of particular diagnostic techniques.

Most experiments are carried out in "ground" facilities which can generate non-equilibrium flows. These facilities generally require important equipment and investment. The essential purpose is to create high enthalpy gas flows undergoing more or less intense perturbations (shock wave, rapid expansion…), so that, physical and chemical processes evolve on a time scale equal to or longer than the characteristic flow time scale.

Two types of facilities are described here, depending on the type of phenomena or the processes analysed, shock tubes and shock tunnels. Thus, if the analysis of the physical and chemical processes themselves is considered as essential, simple facilities, such as shock tubes generating one-dimensional, non-dissipative flows are to be used. On the contrary, if the simulation of the conditions of real flight is required, facilities such as shock tunnels generating hypersonic flow around various bodies must be used.

Other types of facilities generating high enthalpy flows, such as arc tunnels and plasma generators, will not be considered here.

2.0 THE SHOCK TUBE

The simplest model of shock tube consists of creating in a tube of constant (circular or rectangular) cross-section a moving shock wave generating a flow at high temperature and out of equilibrium. Ideally, this flow is one-dimensional and not dissipative [1-6].

2.1 Simple shock tube theory

Schematically, a tube initially containing the test gas (low pressure chamber) is separated by a diaphragm from another chamber (high pressure chamber or driver section) containing another gas (driver gas). After the rupture of this diaphragm the driver gas, acting as a piston expands into the low pressure chamber and generates a shock wave which propagates in the test (driven) gas (Fig.1a). The shock wave gives to the test gas a brutal acceleration accompanied by a jump of temperature, pressure and density. Physical and chemical processes can then start and possibly evolve to their equilibrium state.

The test gas flow is limited by a contact surface (or interface) separating this flow from the driver gas flow (Fig.1b) and, in current installations of a few meters length, this flow generally lasts a few hundreds of microseconds. In the assumed absence of dissipative phenomena, the shock wave preserves a constant speed and, therefore, in a reference frame fixed to this shock wave, the flow is one-dimensional and stationary. Moreover, if the rupture of the diaphragm is assumed instantaneous, a system of centred rarefaction waves develops in the expanding driver gas (Figs.1b and 1c). In addition, the pressure and velocity are preserved through the interface, whereas the temperature and the density undergo a discontinuity.

Report Documentation Page

Form Approved
OMB No. 0704-0188

1. REPORT DATE	2. REPORT TYPE	3. DATES COVERED
SEP 2009	**N/A**	**-**

4. TITLE AND SUBTITLE	5a. CONTRACT NUMBER
Shock Tubes and Shock Tunnels: Design and Experiments	5b. GRANT NUMBER
	5c. PROGRAM ELEMENT NUMBER
6. AUTHOR(S)	5d. PROJECT NUMBER
	5e. TASK NUMBER
	5f. WORK UNIT NUMBER
7. PERFORMING ORGANIZATION NAME(S) AND ADDRESS(ES) **Université dAix-Marseille, France**	8. PERFORMING ORGANIZATION REPORT NUMBER
9. SPONSORING/MONITORING AGENCY NAME(S) AND ADDRESS(ES)	10. SPONSOR/MONITOR'S ACRONYM(S)
	11. SPONSOR/MONITOR'S REPORT NUMBER(S)

12. DISTRIBUTION/AVAILABILITY STATEMENT
Approved for public release, distribution unlimited

13. SUPPLEMENTARY NOTES
See also ADA562449. RTO-EN-AVT-162, Non-Equilibrium Gas Dynamics - From Physical Models to Hypersonic Flights (Dynamique des gaz non- equilibres - Des modeles physiques jusqu'au vol hypersonique)En-Non-Equilibrium Gas Dynamics - From Physical Models to Hypersonic Flights (Dynamique des gaz non- equilibres - Des modeles physiques jusqu'au vol hypersonique)., The original document contains color images.

14. ABSTRACT

15. SUBJECT TERMS

16. SECURITY CLASSIFICATION OF:			17. LIMITATION OF ABSTRACT	18. NUMBER OF PAGES	19a. NAME OF RESPONSIBLE PERSON
a. REPORT	b. ABSTRACT	c. THIS PAGE			
unclassified	**unclassified**	**unclassified**	**SAR**	**26**	

Standard Form 298 (Rev. 8-98)
Prescribed by ANSI Std Z39-18

As well known, the flow parameters of the test gas (region 2) can be deduced from the initial quantities (region 1) and from the shock wave velocity U_s (more exactly the Mach number $M_s = U_s / a_1$). That is why, measurement of the shock wave velocity constitutes the fundamental experimental datum and must be carried out along the low pressure chamber.

2.1.1 Principles of the simple shock tube

We can generally assume that the driver gas behaves as an ideal gas (γ is constant) and that the expansion is an isentropic process in the form of centred waves. This is justified because the driver gas is often a monatomic gas and the temperature is relatively low during the expansion; exceptions are mentioned below.

Thus, across the centred wave system (Fig.1), the quantity $u + \frac{2a}{\gamma - 1}$ (Riemann invariant) remains constant and we have

$$\frac{2a_4}{\gamma_4 - 1} = \frac{2a_3}{\gamma_4 - 1} + u_2 \quad , \tag{1}$$

because $\gamma_3 = \gamma_4$, $u_2 = u_3$ (interface) , and $u_4 = 0$ (high pressure chamber).

We also have

$$\frac{p_4}{p_2} = \left(\frac{a_4}{a_3} \right)^{2\gamma_4 / (\gamma_4 - 1)} \text{ , with } p_2 = p_3 \quad , \tag{2}$$

so that

$$\frac{p_4}{p_2} = \left(\frac{a_4}{a_4 - \frac{\gamma_4 - 1}{2} u_2} \right)^{2\gamma_4 / (\gamma_4 - 1)} \quad , \tag{3}$$

u_2 and p_2 are related to the initial conditions of the test gas (p_1, T_1) by the Rankine-Hugoniot relations. In the frozen case ($\gamma_1 = \gamma_2$), we obtain from these relations and relation (3):

$$\frac{p_4}{p_1} = \frac{\frac{\gamma_1 - 1}{\gamma_1 + 1} \left(\frac{2\gamma_1}{\gamma_1 - 1} M_s^2 - 1 \right)}{\left[1 - \frac{\gamma_4 - 1}{\gamma_1 - 1} \frac{a_1}{a_4} \left(M_s - \frac{1}{M_s} \right) \right]^{2\gamma_4 / (\gamma_4 - 1)}} \tag{4}$$

This expression gives the intensity of the shock wave (M_s) as a function of the initial conditions in both chambers, but under restrictive conditions (ideal gas). That is why it is preferable to determine the flow quantities 2 from the measured velocity of the shock wave, as indicated above. However, the relation (4) gives a qualitatively correct idea of the importance of the various parameters. Thus, in order to obtain the highest possible Mach number, the ratio of initial pressures p_4 / p_1 must be as high as possible, which is

intuitive, but the ratio a_4/a_1 must also be maximum. In particular, when $\frac{p_4}{p_1} \to \infty$, $M_s \to \frac{\gamma_1+1}{\gamma_4-1}\frac{a_4}{a_1}$.
Thus, for a given test gas, we see the interest to use a light and hot gas as a driver gas. We can also deduce from the relation (4) the maximum expected values for M_s in the case of a given gas pair.

These results are only qualitative if chemical processes are significant behind the shock. Thus, the shock Mach number must be generally deduced from assumed equilibrium conditions behind this shock, and of course, the maximum values for M_s are lower than those given by the expression (4).

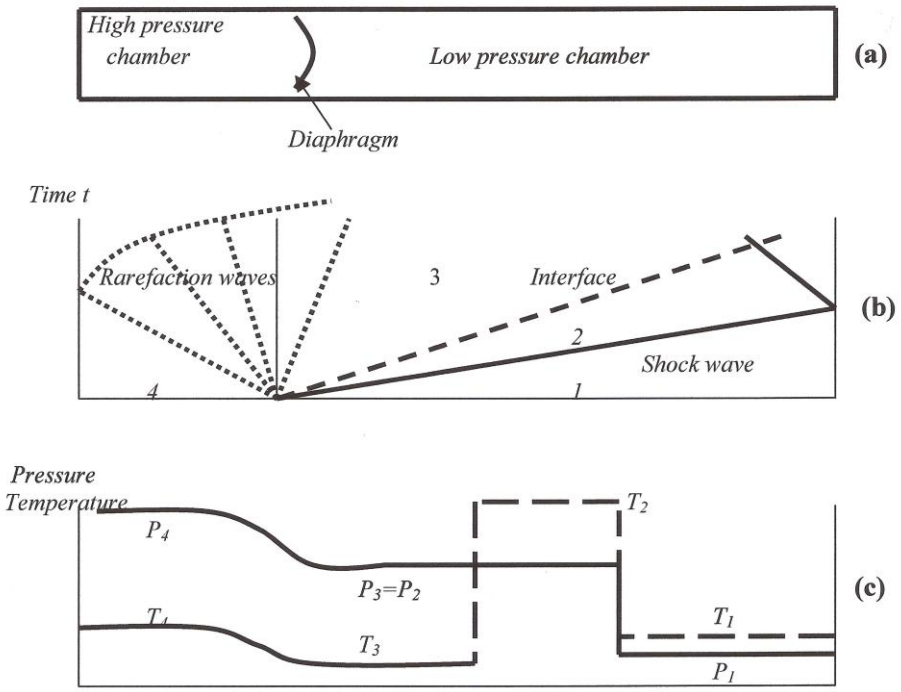

Figure 1: Shock tube : Principle and operation

(a) :Simple shock tube

(b) :Wave system in a shock tube

(c) : Pressure and temperature distribution at a given time t

2.1.2 Technological limitations and constraints

As already discussed, the test gas flow between the shock wave and the interface has a very short duration, and it can be disturbed by the various wave systems which propagate in the tube because of its limited dimensions. Thus, the rarefaction waves going up in the driver section after the rupture of the diaphragm are reflected at the end of this chamber and come back (while accelerating) until possibly overtaking the interface and the test gas. Similarly, the incident shock wave may be reflected at the end of the tube and may interact with the incident test gas flow: this last point is not always a disadvantage (see below). However, if we take into account these configurations, it is of course possible to optimise for example the duration of the test gas flow at a given abscissa along the tube (at the test section for example), independently of the disturbing phenomena described hereafter.

2.2 Disturbing Effects

Obviously, this ideal scheme of operation corresponds only roughly to reality and various phenomena contribute to somewhat modify this scheme and have an influence on the analysed non-equilibrium phenomena. The most significant effects concern the perturbations related to the presence of the wall boundary layer and, to a lesser extent, those coming from the non-instantaneous rupture of the diaphragm.

2.2.1 Wall boundary layer

The boundary layer which develops along the walls of the shock tube between the incident shock and the interface, acts like a well for the non-dissipative part of the test gas and a loss of this gas occurs through the interface in the boundary layer (Fig.2)since the boundary layer of the driver gas has a negligible thickness (high value of the Reynolds number *Re* due to the low temperature and high density). This leads to a deceleration of the shock wave, an acceleration of the interface and thus a non-constant value of the flow quantities. This unsteady regime tends to a stationary limiting regime theoretically obtained when the total mass flux through the shock wave is equal to that lost through the interface inside the boundary layer. This last mass flux increases because the separation distance between the shock wave and the interface initially increases (Fig.1). The shock wave and the interface in the limiting regime, have the same (constant) velocity, but the flow quantities, while being stationary, vary between the shock and the interface.

An example of calculation of the trajectories of the shock wave and the contact surface is represented in Fig.3, in the case of a low initial pressure for which the boundary layer is laminar [7-9]. For higher values of the initial pressure, the boundary layer is turbulent but approximate models are available [10,11].

These effects are all the more significant as the initial pressure and the cross- section of the tube are lower (low value for *Re*). Moreover, the hot gas loss across the interface tends to create a pressure gradient normal to the wall and therefore tends to give to the interface an increasingly convex form.

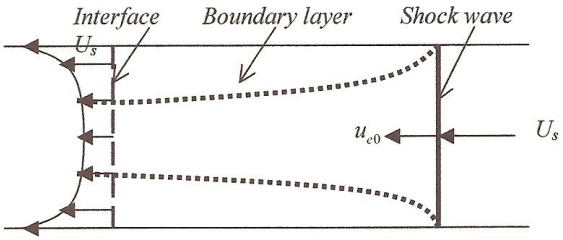

Figure 2: Scheme of flow in a shock tube

(Coordinate system fixed to the shock wave)

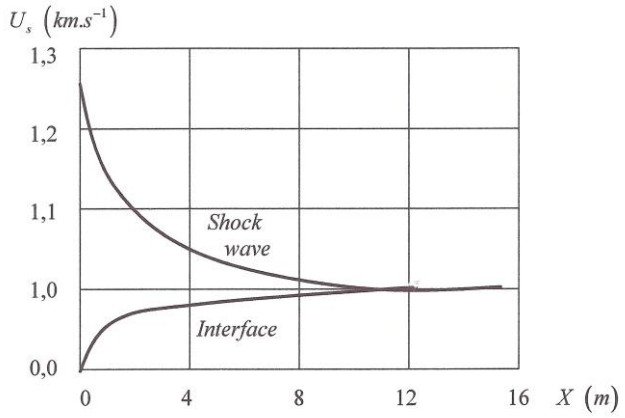

Figure 3: Spatial variation of the shock wave and the interface

(Driver gas : Helium , test gas : Argon : p_1=132Pa, T_1=293K, M_{si}=4)

2.2.2 Non-instantaneous opening of the diaphragm

In a 'real' shock tube, the shock wave is not instantaneously created but is formed by the coalescence of the compression waves arising during the progressive opening of the diaphragm and thus accelerates little by little a "long time" after the complete opening. Several meters of tube are often required to obtain a shock at constant speed.

There are various models of this acceleration phase which simultaneously take into account the mechanical opening process, the presumably isentropic and stationary flow through the aperture, the recompression stationary shock and successive compression waves propagating downstream and progressively accelerating the shock wave [12]. Thus, knowing the total duration of the diaphragm opening, the initial pressure ratio of the driver gas and of the test gas, and their composition, it is possible to describe the acceleration phase of the shock wave and the related properties of the flow [13,14]. The shock wave is thus strongly accelerated close to the diaphragm until reaching a maximum speed, then it slows down slowly up to the ideal value [15] given by relation (4) (Fig.4). The acceleration phase is all the shorter as the ratio of the initial pressures is higher, as the driver gas is lighter and as the total opening time t_{ouv} is shorter.

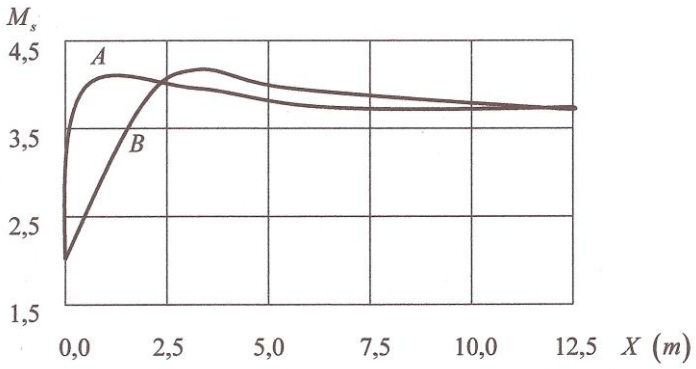

Figure 4: Influence of the opening time of the diaphragm on the evolution of the shock wave

(air/air, p_4/p_1 =17700, A: t_{ouv}=300µs, B: t_{ouv}==600µs)

2.2.3 Combined effects of boundary layer and diaphragm opening

The result of the simultaneous action of the preceding effects consists in an initial acceleration of the shock wave followed by a continuous deceleration. The predominance of one or the other effect depends on the experimental conditions. An example of computational result of the spatial variation of the shock wave is presented in Fig.5 [16], and is compared with an experimental evolution [17]. We can observe a drastic variation due to the low initial pressure and the use of air as a driver gas. This variation is naturally less marked for more "usual" conditions (higher initial pressure, light driver gas…).

2.2.4 Transition in the boundary layer

The laminar-turbulent transition may be determined with heat transfer gauges [18] placed flush with the wall and therefore sensitive to the boundary layer regime.

With several gauges placed along the shock tube it is possible to follow the evolution of the transition point [19]: We observe that it strongly depends on the Reynolds number per unit length Re_l: thus, for low values of Re_l, the transition appears in the form of large structures called 'turbulent spots' which are regularly created along the tube and which regress towards the contact surface (Fig.6a). For higher values of Re_l , the size of the disturbances decreases and their frequency increases, so that a compact transition front appears little by little and moves at the same speed as the shock (Fig.6b).

A precise and general stability criterion is difficult to define, but regimes of global stability can, for each type of installation, be experimentally defined, apparently independently of the shock wave Mach number [19].

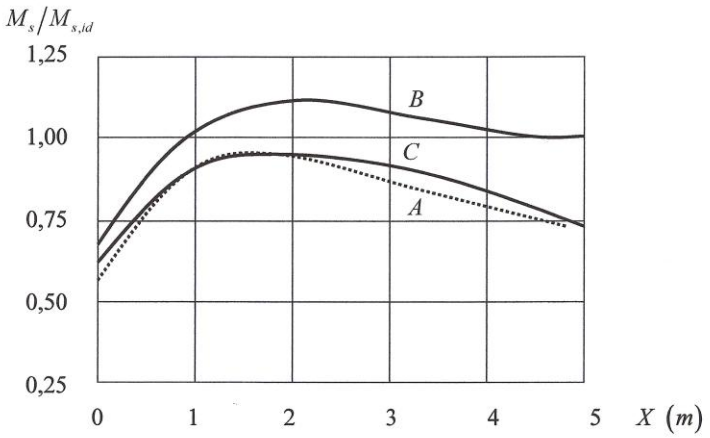

Figure .5: Example of a shock wave profile

(air/air, p_4/p_1 =2134, p_1=526Pa, t_{ouv}=618µs)

A : Experimental, B : Computation without boundary layer,

C : Computation with boundary layer

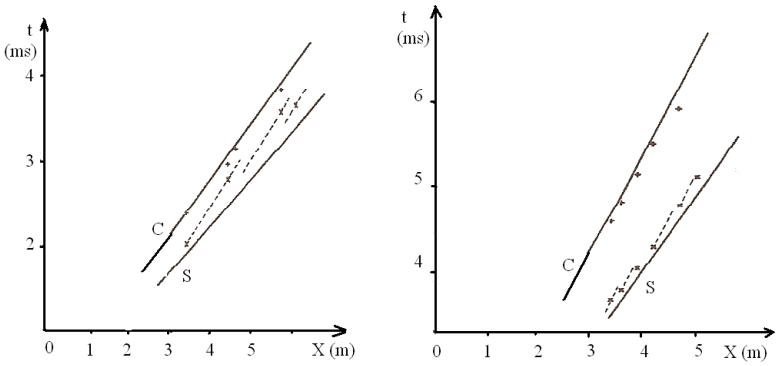

a **b**

Figure 6: Experimental evolution of the transition in a shock tube

(S : Shock wave, C : Contact surface (+), x : Transition)

a : M_s =5,7; p_1 =921Pa; Re_1 =64.10^4 m^{-1}

b : M_s =3,8; p_1 =6934Pa; Re_1 =406.10^4 m^{-1}

2.3 Reflected Shock Waves

2.3.1 Generalities

At the end of a closed tube, the shock wave is reflected and comes back into the gas already compressed and heated by the incident shock wave. So there is a further increase of temperature, pressure and density of the test gas, which, in principle, gives more favourable conditions to start chemical processes. Moreover in theory, the gas is without velocity behind the reflected shock waves.

Of course, the gas parameters of this region (frozen or in equilibrium) may be computed with the usual Rankine-Hugoniot relations across the reflected shock wave in a coordinate system fixed to this wave. If the ideal gas model is used, we obtain analytical relations for the pressure and temperature ratios across the shock as well as for the reflected shock velocity as functions of p_2/p_1. This pressure ratio itself is simply related to the incident shock Mach number M_s. For a "real" gas (in equilibrium), the values obtained for p_5 and T_5 are of course lower.

2.3.2 Disturbing effects

As in the case of the incident shock, various aerodynamic processes can disturb the test gas downstream from the reflected shock.

One of the disturbing effects relates to the interaction of the reflected shock and the contact surface: this interaction is summarized in Fig.7.

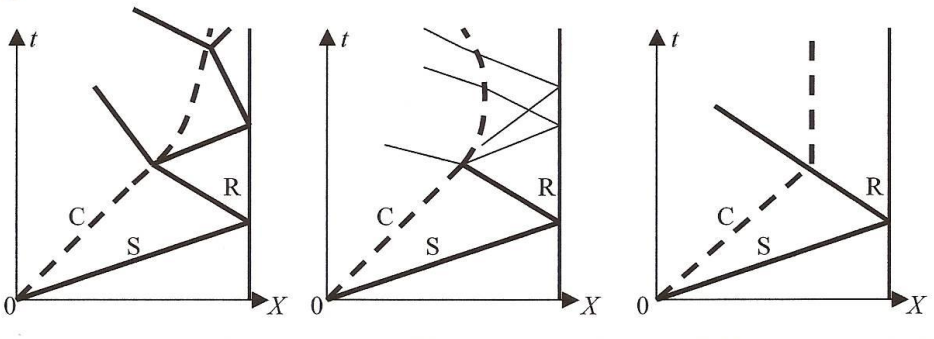

a **b** **c**

Figure 7: Wave systems generated by the interaction of the reflected shock and the interface

a : Over-tailored case, **b** : Under-tailored case, **c** : Tailored case

Three interaction cases are possible, either the reflected shock is partially reflected on the interface in the form of shock (case a), or in the form of rarefaction waves (case b), or it crosses the interface without reflection (intermediate case c). In the three cases, a shock wave propagates into the driver gas. In the first two cases, which are the most frequent, the properties of the test gas downstream from the reflected shock are modified and the useful test time can be strongly reduced, whereas it is theoretically very large in the third case for which the interface is stopped ("tailored case"). This occurs however only for quite precise initial conditions (for example, for $M_s = 6$ in the case of a gas pair He / N_2) [20]. However, of course, if chemical processes are to be analysed behind the reflected shock, the tailored case represents the best experimental condition.

This scheme itself is disturbed by the presence of the boundary layer developing along the side walls downstream from the incident shock [21]. Under the action of the reflected shock, this boundary layer tends to separate from the wall (too low stagnation pressure), and a gas "bulb" is created on which the reflected shock adopts a structure in λ (Mach reflection). This phenomenon (Fig.8) is all the more accentuated as the gas atomicity is high (small γ value, Fig.15). Then, the propagation of the reflected shock is obviously affected and, across the "feet" of the λ shock, there remains a gas velocity component directed towards the end of the tube. This disturbs (primarily cools) the test gas. Moreover, when the reflected shock encounters the interface, the driver gas itself flows along the side walls, preceding the central part, which is experimentally confirmed [22].

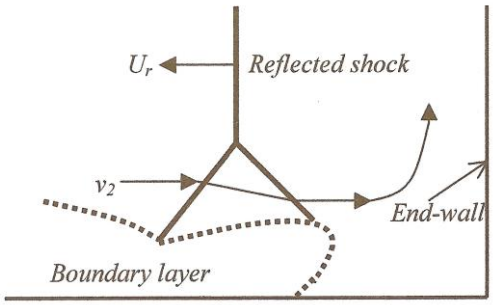

Figure 8: Scheme of interaction reflected shock-boundary layer

2.4 Configurations and Operation

2.4.1 General design features

As described above, the 'simple' shock tube composed of two chambers represents the majority of the existing installations. However, these installations differ according to the type of studies planned. Thus, for example, the tubes with circular cross-section, which are easier to construct, lend themselves less easily to visualizations than those with square or rectangular cross-section. Moreover, these require a transition section between the high pressure (HP) chamber (of circular cross-section for safety reasons) and the low pressure (LP) chamber.

As already discussed, the length of both chambers is important to optimise the flow test time because of the various wave systems and end-wall reflections. Moreover, a third chamber large-sized and placed downstream from the low pressure chamber is often used when the experiments are limited to the flow downstream from the incident shock. This chamber (dump tank), separated by a second diaphragm from the driven section and in which high vacuum conditions prevail , makes it possible to obtain after the end of experiments a low residual pressure, useful in case of high pressure and/or combustible driver gases (H_2) or in case of toxic test gases (CO, CN…).. The residual initial pressure, obtained after pumping, especially in the test section must be sufficiently low (10^{-2}-$10^{-4}Pa$) to have no influence on the purity of the test gas, in particular for spectroscopic studies.

The diaphragms separating HP and LP chambers are generally metallic, aluminium or copper, for moderate pressures in the HP chamber (lower than 10^7Pa), steel for higher pressures. They can be in plastic material for lower pressures. The metallic diaphragms are scored (cross-shaped scores with variable depths of $1/2$ to $2/3$ of their thickness) and calibrated to open at well defined pressures. We thus obtain a dispersion of the incident shock Mach number which does not exceed 1%. Generally, for moderate pressures, the diaphragms break themselves by increasing the pressure of the HP chamber. For more precision, and especially in the case of very high pressures, a double diaphragm system is used : it consists of a small chamber inserted between the HP and LP sections and in which the pressure is intermediate between those of these two chambers. The sudden pumping of this chamber produces a precise and reproducible bursting of the diaphragms for given conditions.

2.4.2 Configurations. Performances

Various possibilities exist to improve the performances of the simple shock tube, i.e. to increase the incident shock Mach number: these possibilities are briefly described below. Most of them are put into practice.

- Area reduction close to the diaphragm

The HP chamber has a section larger than that of the LP chamber: there is a quasi stationary expansion of the driver gas in the area transition zone, which increases the efficiency of the thrust. We can define a parameter *g* equal to

$$g = \frac{\left(p_4 / p_1 \right)_{A_4/A_1 = 1}}{\left(p_4 / p_1 \right)_{A_4/A_1}} \quad ,$$

(5)

so that the tube with variation of cross-section is equivalent to a tube of constant cross-section working with an initial pressure ratio equal to $g.p_4/p_1$, and an initial sound velocity ratio equal to

$$a_4/a_1 . g^{(\gamma_4 - 1)/2\gamma_4} \qquad (6)$$

It should be noted that the increase in Mach number is significant [6].

- Double–diaphragm shock tube

A third section is added to the LP chamber and is used as the test section. It is separated from the intermediate chamber by a diaphragm on which the shock wave is reflected before breaking it, thus creating conditions of high pressure and temperature in the gas of this chamber. This gas is used as a driver gas for the test gas of the third section. In this case, the Mach number is significantly higher but the test time is greatly reduced.

It is also possible to use the expanded gas of the intermediate chamber as the test gas in super or hypersonic regime [23].

- Combustion shock tube

The increase of the sound speed in the driver gas can be obtained, not only by using a light gas, but also by raising its temperature. One efficient way is to create a combustion in the HP chamber.

This combustion is generally obtained by using a stoichiometric mixture of hydrogen and oxygen diluted in helium (approximately 70%). The main difficulty consists in obtaining a uniform combustion without detonation; this is generally realized with a significant number of spark plugs arranged in spiral along the HP chamber. The gain in Mach number however is partially compensated by a stronger deceleration of the shock wave due to the sharp pressure fall after the combustion and also sometimes to a rebound of the “petals” of the diaphragm on the side walls.

An alternative solution precisely consists of creating a detonation wave close to the diaphragm and which propagates upstream in the HP chamber: it results in a better uniformity for the pressure and temperature in the driver gas after the rupture of the diaphragm [24].

- Free piston shock tube

. The fast compression of a light gas represents also a means for increasing the pressure and the temperature of this gas, used as a driver gas. This compression is carried out by a piston launched at high speed in a tube serving as a compression chamber: the compressed hot gas ensures the rupture of the diaphragm. This method undoubtedly represents the most efficient process to create a shock wave of high intensity [25].

A diagram of this device is represented in Fig.9. In a first chamber (tank R), a gas (generally air) is compressed up to several hundreds of atmospheres and, owing to a double diaphragm system D1-D2, pushes a piston P (10 to 500 *kg*) which compresses the driver gas (generally helium or helium-argon mixture) of the HP chamber. The diaphragm D3, which must be initially calibrated, located at the end of this chamber is then ruptured creating a shock wave in the LP chamber. After the rupture, the piston continuing to move maintains a pressure sufficiently high to delay the propagation of rarefaction waves towards the LP chamber.

Of course, the piston must be rapidly stopped for safety reasons and also to avoid a rebound [26-28].

In addition, special configurations of the piston are used to have a continuous rise of the pressure at the end of the HP chamber and thus to obtain a reproducible rupture of the D3 diaphragm. An example of operation, in form of an (*x*, *t*) diagram, (trajectory of the piston, wave systems) is presented in Fig.10

Important shock Mach numbers (10-25) are thus generated in gases or gas mixtures representative of various planetary atmospheres

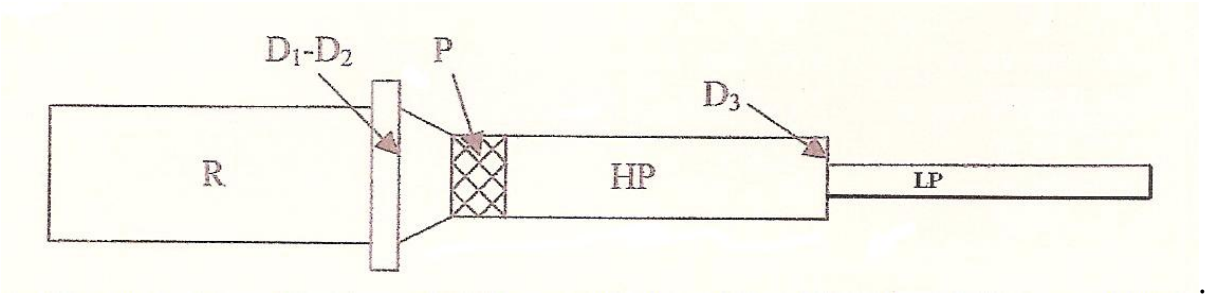

Figure 9: Diagram of a free piston shock tube

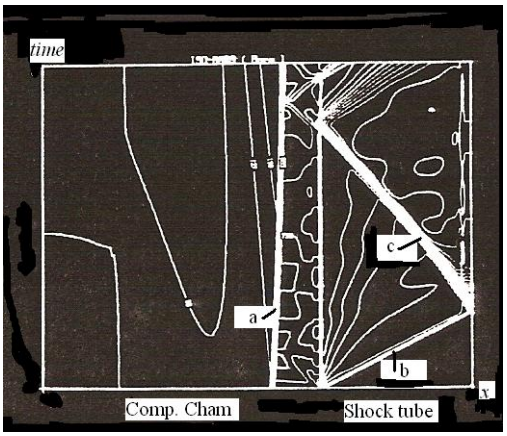

Figure 10: (x, t) velocity diagram in a compression chamber and a shock tube

(a: Piston, b: Incident shock wave, c: Reflected shock wave)

2.5 Usual Experimental Measurements

The measurement methods of the usual flow parameters such as pressure, density, heat flux and visualization techniques are illustrated here by a few examples.

2.5.1 Pressure measurements

An example of pressure recording behind a reflected shock wave is presented in Fig.11 (piezoelectric gauge).

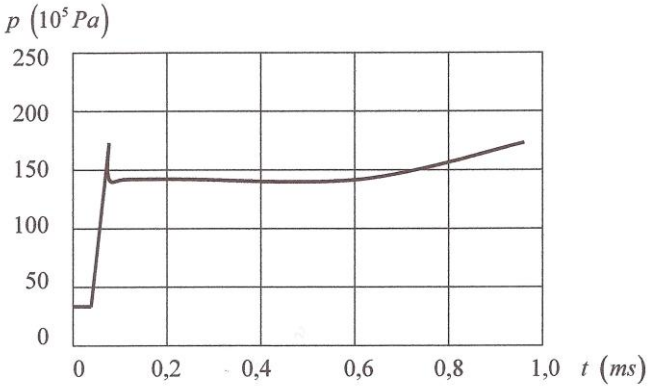

Figure 11: Pressure record at the end-wall of a shock tube (with filter)

2.5.2 Heat flux measurements

An example of wall temperature evolution given by thin film platinum heat gauges mounted flush with the wall is given in Fig.12. Heat flux can be deduced from this type of recording.

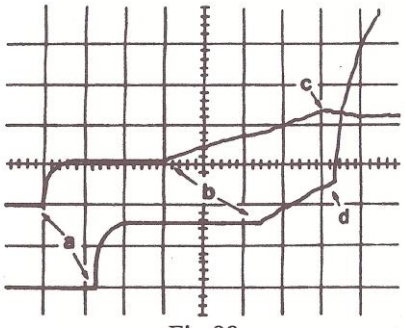

Figure 12:. Oscillogram of wall temperature in a shock tube (200μs/div. **)**

(a : Incident shock wave, b : Transition, c : Interface, d : Reflected shock)

2.5.3 Density measurements

The fringe system across a shock wave obtained with a Mach-Zehnder interferometer is shown in Fig.13: the vibrationally relaxing zone is clearly visible (N_2, M_S=6).

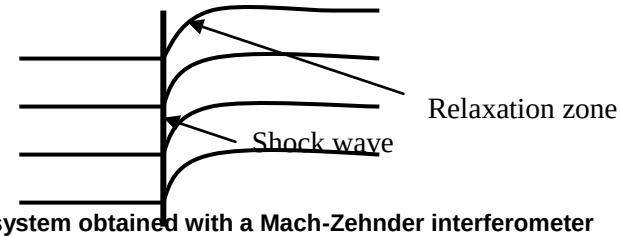

Figure 13: Fringe system obtained with a Mach-Zehnder interferometer

2.5.4 Visualizations

Visualizations can be carried out by interferometry, as seen above. They are then quantitative (density measurements). More qualitatively, the significant and different deviation of light rays crossing the shock tube by flow regions of different densities gives the possibility to visualize the flow areas presenting density gradients, in particular the shock waves. This is the Schlieren technique also associated with fast photography or cinematography [(x, t) or (y, t) diagrams]. Examples of shock tube flows are thus represented in Figs.14 and 15 [30].

(**a**) (**b**)

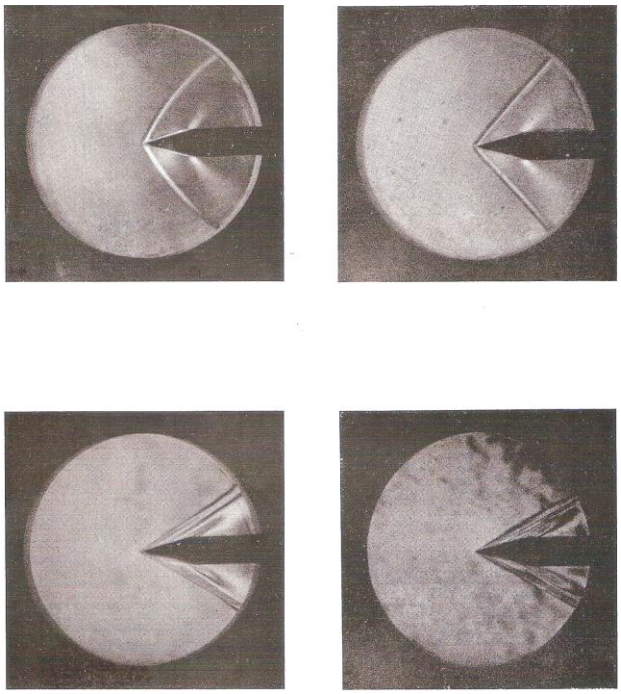

(**c**) (**d**)

Figure 14: Flow around a wedge (semi-angle 15°)

(air-air, M_s =3,86, p_1 =130Pa)

(θ : Instant after the passage of the shock wave),

(a): θ= 23μs, (**b**): θ= 100μs, **(c)**: θ=700μs , **(d)**: θ=1300μs

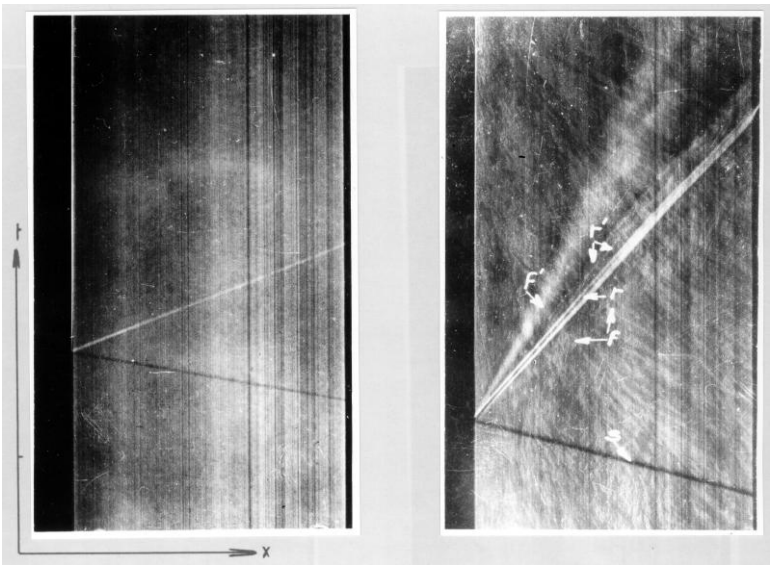

(**a**) (**b**)

Figure 15: Reflection of a shock wave at the end-wall of a shock tube (x,t diagram)

(**a**) : Argon, M_s =3,30, p_1 =790Pa ; (**b**) : Carbon dioxide, M_s =3,40, p_1 =1315Pa

s : Incident shock, r : Reflected shock, r' : Secondary shocks,

f : Front of the bifurcated shock, f' : Rear of the bifurcated shock

3.0 THE SHOCK TUNNEL

As specified in the introduction, the generation of non-equilibrium flows can be also realized with a high pressure hot gas, assumed to be in equilibrium, then quickly expanded in a nozzle in order to obtain an hypersonic flow at low temperature but in chemical and/or vibrational non-equilibrium. The shock tunnel represents one of the main facility of this type.

3.1 Principles

The principle of the shock tunnel is derived from the shock tube concept. Thus, the gas downstream from the incident shock wave can be directly expanded in a nozzle placed at the end of the shock tube. The flow can then become hypersonic at the exit of the divergent part of the nozzle. However, this process is seldom used for various reasons, primarily because of the very short test time. It is preferable to use the gas downstream from the reflected shock as a reservoir gas. In theory it is at rest, in equilibrium and at high temperature and pressure during a relatively long time in the "tailored" conditions (section 2.3.2). Thus at the exit of the nozzle, we can expect test times of about one millisecond. The main drawbacks arise from the possible pollution of the test gas by the premature arrival of the driver gas (section 2.3.2) and from the "starting process" of the nozzle requiring a non-negligible time. Thus, the duration of the "useful" (stationary) test time is only a few hundreds of microseconds, even for relatively large installations. The diagram of a free piston shock tunnel is represented in Fig.16.

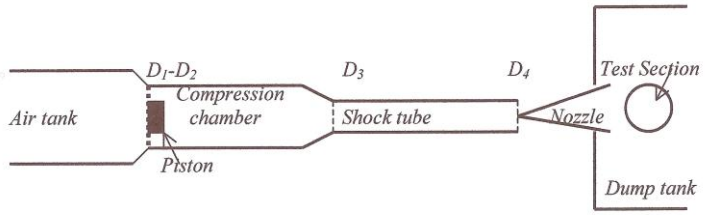

Figure 16: Scheme of a free piston shock tunnel

3.2 Operation

At the rupture of the diaphragm D4, a shock wave propagates in the nozzle, compressing the residual gas of the expanding chamber (dump tank) initially at very low pressure. Another shock wave, known as a secondary shock, is formed downstream to ensure the continuity of pressure with the test gas expanding into the nozzle. This shock interacts with the very thick boundary layer of the residual gas (Mach reflection) but is pulled downstream by the test gas flow, the stationary expansion phase of which constitutes the useful part of the flow.

The traditional nozzles, known as "contoured" or "adapted", used in supersonic ideal gas flow are difficult to use in hypersonic non-equilibrium flows, because they are in fact, "adapted" only for conditions close to one single point of operation. Thus, they are generally replaced by nozzles including a conical divergent part. These nozzles require a suitable convergent-divergent connection but they are simpler to build and more easily calculable. However, they also suffer from some defects ("source effects").

3.2 Calibration

Measurements of stagnation pressure (Pitot pressure) with small probes placed normally to the flow are used to validate flow computations and to determine the non-dissipative part of the test section, in particular at the exit of the nozzle, where the models are placed. An example of distribution of Pitot pressure [31] is presented in Fig.17. This pressure is practically insensitive to non-equilibrium and physical models. These measurements may also give an idea of the effective duration of the useful test time.

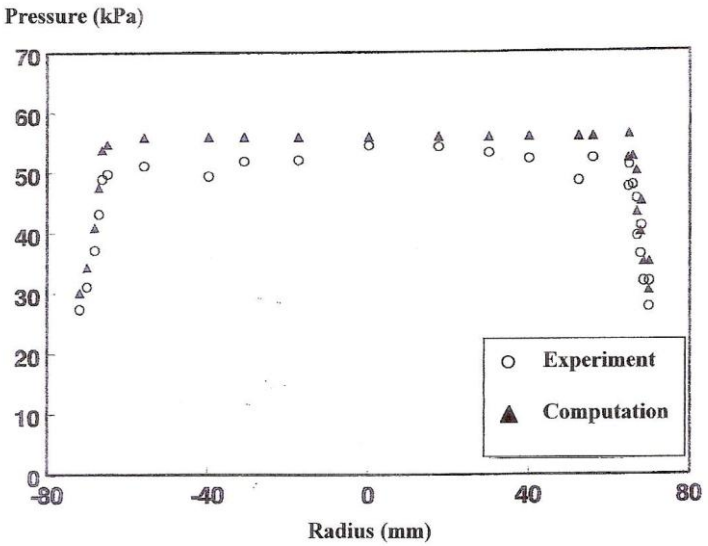

Figure 17: Pitot pressure distribution at the exit of a nozzle

(p_0=18MPa, T_0=6000K, M_∞=7,2)

Measurements of static pressure and of wall heat flux generally complete the knowledge of the nozzle flow. Thus, an example of the distribution of the wall pressure for an air flow along an hypersonic nozzle is represented in Fig.18 [32] and is compared with the pressure calculated by taking into account the non-equilibrium and by assuming that the boundary layer is laminar.

Similarly, an example of the wall heat flux distribution along the same nozzle [32] is represented in Fig.19. The flux decrease observed along the nozzle approximately corresponds to that computed with a laminar boundary layer. However in the distribution, we observe local increases, similar to those observed in a shock tube and which correspond to the appearance of turbulent spots which are quickly spreading: this would also correspond to the longitudinal variation of the Reynolds number which, initially growing (because of the increasing distance) reaches a maximum then decreases very quickly mainly because of the decreasing density, so that it is difficult to find here a well definite transition.

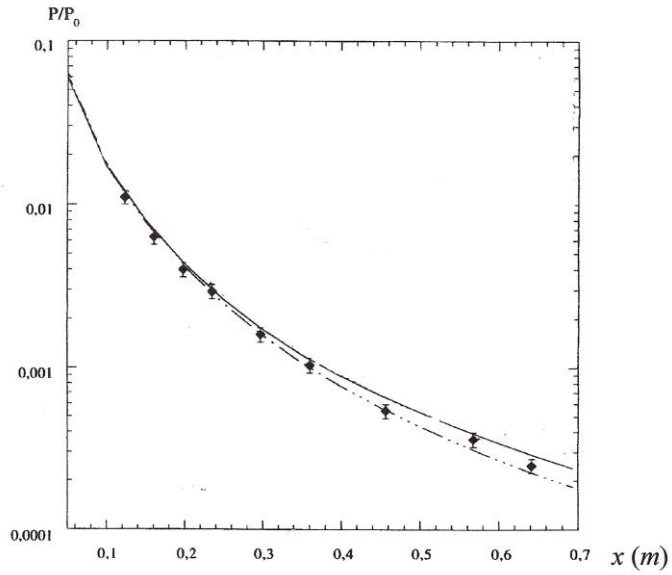

Figure 18: Static pressure distribution along an hypersonic nozzle

(Conical nozzle, length : 70cm, semi-angle : 8°, $A/A_c = 164$)

(Air, $M_s = 8.75$, $p_0 = 45.10^6$Pa, $T_0 = 6500$K) • : Experimental points

—— : Computation with vibrational coupling, – – – : Computation without coupling

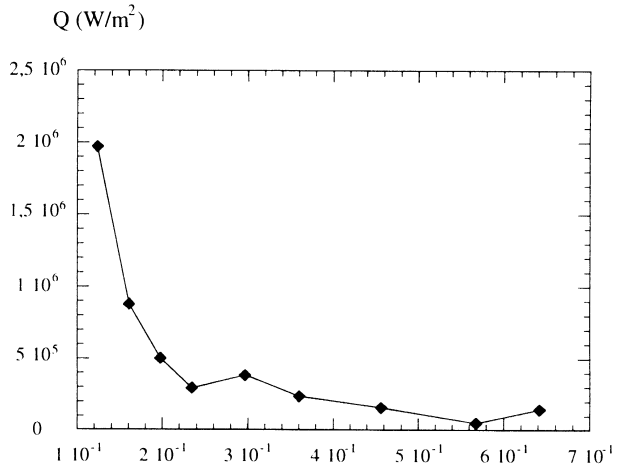

Figure 19: Wall heat flux distribution along an hypersonic nozzle

(Nozzle of the figure 18), (Air, $M_s = 5.76$, $p_0 = 23.10^6$Pa, $T_0 = 3530$K)

• : Experimental points

4.0 TYPICAL EXPERIMENTS

A few examples of the main two types of processes studied in shock tube and shock tunnel are briefly presented and discussed hereafter: they are related to vibrational relaxation and chemical kinetics in homogeneous phase. Other important phenomena in non-equilibrium media such as catalytic properties, ionisation or combustion processes widely analysed in shock tube and shock tunnel are not described here.

4.1 Vibrational Relaxation

The purpose of most measurements is to determine the global relaxation times defined by using the Landau-Teller model [33], since this model is widely used in the computer codes of hypersonic flows. These include TV relaxation times for pure gases, TV and VV relaxation times for mixtures. The purpose of more precise measurements is the determination of the transition probabilities and also the evolution of the vibrational populations in the relaxation zone downstream from a shock wave (incident or reflected), thus providing a comparison with theoretical models.

4.1.1 Relaxation times. Methods and results

The determination of global relaxation times is essentially carried out in shock tube. For pure gases, the system of Rankine-Hugoniot equations is used, coupled with the Landau-Teller equation in which the relaxation time τ_V is regarded as unknown. The measurement of one macroscopic parameter is thus in theory sufficient to determine $\tau_V\left(p,T\right)$ at each point of the zone of relaxation: The most sensitive quantities to the non-equilibrium and the most convenient to measure are the density ρ and the total vibrational energy E_V.

Density measurements are made by interferometry (section 2.5.3) and the density profiles in the non-equilibrium zone are deduced from the fringe system.

The vibrational energy is deduced from the intensity of infra-red emission due to the rotation-vibration lines of heteropolar molecules having a permanent dipole such as *CO*. Thus, the intensity emitted by all the monoquantum transitions (fundamental) is proportional to the global average vibrational energy and the biquantum transitions (overtone) give a signal proportional to the square of this energy. An example of the time evolution of the intensity of the bands centred on 4.6 μ and 2.3 μ, corresponding respectively to the fundamental and the overtone coming from the flow downstream from a shock wave in *CO* is represented in Fig.20. A calibration of the equipment is necessary because the IR detector is sensitive to the emitting region before the arrival of the shock wave in the test section as it is visible in Fig.20 (curve A). The time evolution of E_V is deduced from these recordings.

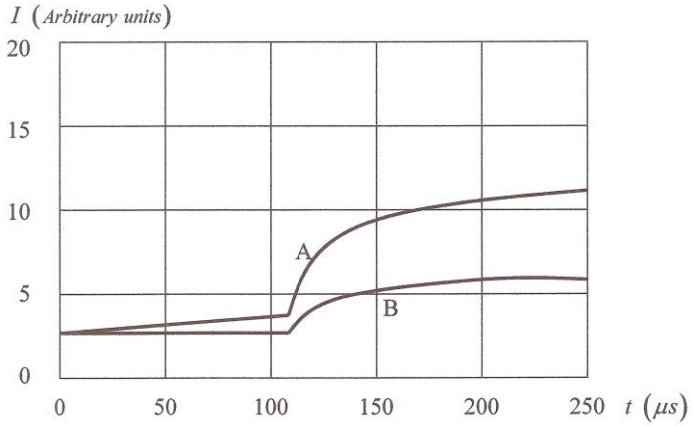

Figure 20: Infrared emission signals in CO
(M_s =5.63, p_1 =2500Pa), A : Fundamental ; B : Overtone

The representation of the results is based on the LT-SSH model (Landau-Teller-Schwartz-Slavsky-Hertzfeld) which leads to the following approximate dependence of $\tau_V p$ on *T*.

$$\tau_V p \propto F(T)\exp\left(T^{-1/3}\right) \quad , \tag{7}$$

where $F(T)$ depends weakly on T, so that we can write

$$Log\left(\tau_V p\right) = AT^{-1/3} + B$$

Thus, if Z_1^0 is the probable number of TV collisions necessary for the de-excitation of the molecules in the first level and *Z* is the collision frequency, we have

$$Z_1^0 = \tau_V Z \propto g(T)\exp\left(T^{-1/3}\right) \tag{8}$$

Representations of Z_1^0 are given in Fig.21. It must be pointed out that the LT-SSH theory is essentially valid in the temperature range between 1000 and 5000K.

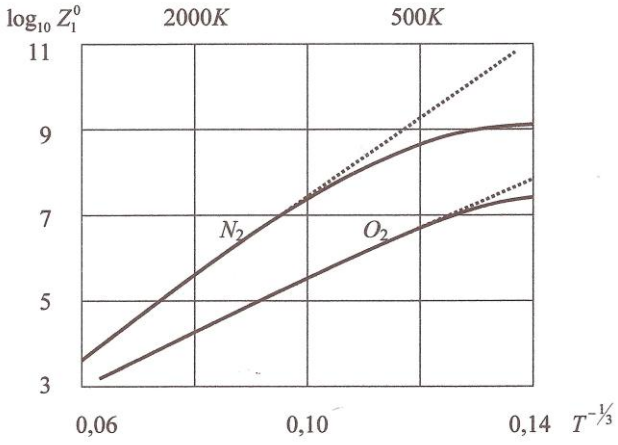

Figure 21: LT-SSH representation for N_2 and O_2
——: Experiments, ·····: SSH

Many other results on pure gases and mixtures are available [34].

4.1.2 Vibrational populations

- Experiments in shock tube

The evolution of the vibrational populations does not generally take place according to a Boltzmann distribution and consequently the concept of vibrational temperature has not physical meaning. Thus, it is preferable to determine these populations directly by experiment. The measurements are essentially made in two ways, either by spontaneous Raman diffusion or by infrared absorption.

When molecules initially in the levels i_v and i_{v+1} are excited by a radiation of frequency ν and intensity *I*, they reemit diffusion lines of frequency $\nu-\Delta\nu$ (Stokes lines) and $\nu+\Delta\nu$ (Antistokes lines), with respective intensities I_S and I_{AS} such that

$$I_S / I \propto n_{i_v} \qquad\qquad I_{AS} / I \propto n_{i_v+1}$$

The recording of these quantities in the relaxation zone gives the possibility to follow the evolution of the populations n_{i_v} and n_{i_v+1} , with a calibration operated in the equilibrium region. A powerful light source is necessary and, generally, only levels 0 and 1 (usually the most populated) are accessible. Values of Z_1^0 represented in Fig.21 are deduced from this type of measurement.

The absorption coefficient α of a medium made up of heteropolar molecules and crossed by a spectral line corresponding to a transition $i_v,\ i_r \to i_v+1,\ i_r-1$ (*P* branch) depends on the population of the levels concerned [35,36], so that from the measurement of two coefficients α_{i_r,i_v} et α_{j_r,i_v} it is possible to deduce the populations of the levels i_v et i_v+1, since we have

$$\begin{aligned} n_{i_v} / n &= A_1\alpha_{i_r,i_v} + B_1\alpha_{j_r,i_v} \\ n_{i_v+1} / n &= A_2\alpha_{i_r,i_v} + B_2\alpha_{j_r,i_v} \end{aligned}$$

(9)

In this system, the four coefficients A_1, A_2, B_1 and B_2 depend on spectral parameters, generally well-known, and on macroscopic flow parameters $(T,\rho,\ldots)$. The flow parameters depend very little on the vibrational distribution model , so they are calculated before solving the system (9), assuming for example a LT-SSH model. A typical evolution of vibrational populations is given in Fig.22.

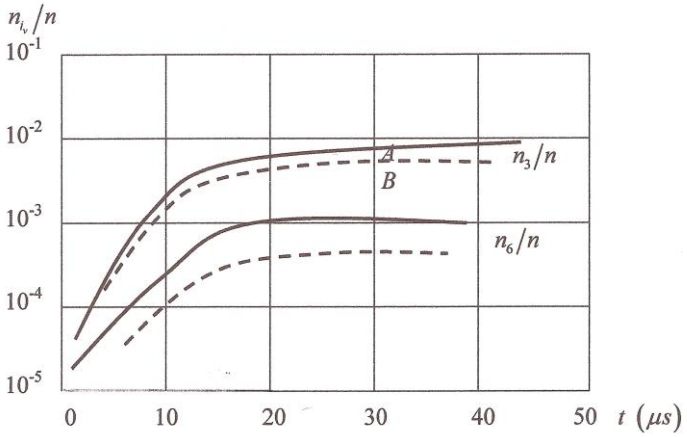

Figure 22: Evolution of the relative population of the 3rd and the 6th vibrational level

$(CO\ ;\ M_s=5{,}60;\ T_1=293K;\ p_1=196Pa\ )$,

_____ : Experimental, Treanor , _ _ _ _ : Boltzmann

- Experiments in shock tunnel

One of the main difficulties of measurements at the nozzle exit of shock tunnels comes from the low density of the flow, which constitutes the price to pay for the generation of an hypersonic flow. Thus the techniques used in shock tubes are not efficient. That is why, the methods used in the past to determine the global relaxation times were indirect measurements (sodium or chromium line reversal, inclusion of tracers, Rayleigh diffusion…). The general conclusions of these studies were that the vibrational relaxation times deduced from these measurements were much lower than those deduced from measurements in shock tubes and thus, that the flow at the nozzle exit was much closer to equilibrium than that calculated using the values of relaxation times determined in shock tube [37].

As no plausible explanation could justify these results, recently direct measurements of vibrational populations in nitrogen were realized by spontaneous Raman diffusion [38] and the distribution obtained from these measurements clearly show that this distribution for the first three levels is close to a Boltzmann distribution at the frozen vibrational temperature corresponding to the temperature given by a Navier-Stokes-Landau-Teller calculation including values for relaxation times measured in shock tube. Similar results have been obtained in another installation [39]. Therefore, independently of the experimental uncertainties (relatively important), no significant difference appears between the relaxation times determined in compression and in expansion regimes. Impurities, however, may have a significant influence on the population of higher levels.

4.2 Chemical Kinetics

Many chemical reactions have been studied in shock tubes but most results suffer from measurement techniques, often indirect (interferometry…), or incomplete (emission or absorption…) used in the past. The consequence is a large dispersion of these results also due to the methods for data reduction. Now, new measurement techniques and data interpretations enable us to obtain more reliable results.

Thus, the time-resolved emission spectra of particular species downstream from a shock wave can allow, not only to ascertain the kinetics of formation or destruction of these species, but also to validate (or not) complex calculations of chemical kinetics in which these species are involved. The recording of these spectra (or parts of spectra) during one single experiment, constitutes obviously a significant progress compared to the recordings of one or a few particular lines, as often made in the past.

An example of such an experiment is represented in Fig.23. The radiation emitted by the shocked gas is focused to a monochromator equipped with a high resolution holographic grating. At the exit, a streak unit equipped with a CCD camera gives the possibility to record a significant part of the analysed spectrum [40].

The mixture is composed of $92\%N_2$, $3\%CH_4$, $5\%Ar$ (simulation of Titan atmosphere); behind an incident strong shock wave, numerous reactions take place including the production of the radical *CN* emitting an intense violet band spectrum arising from an electronic transition including vibrational bands: among them, the $\Delta v = 0$ sequence (Fig.23) has the strongest intensity.

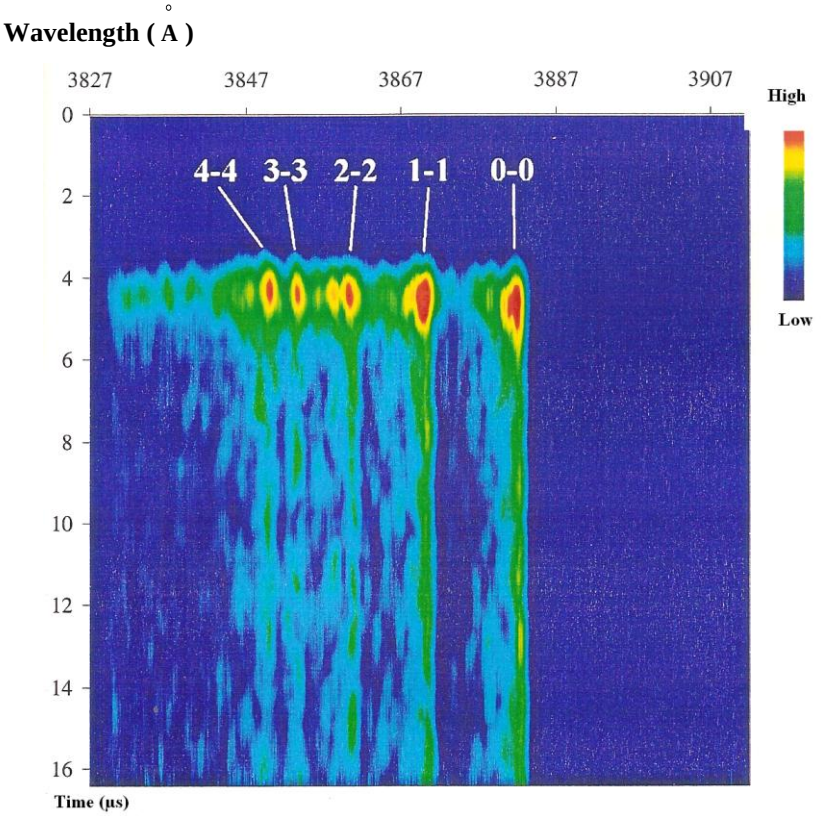

Figure 23: Example of streak image ($\Delta v = 0$ ***CN*** band of the mixture $CH_4 / N_2 / Ar$ **)**

(U_s=5560m/s, p_1=220Pa)

From this type of spectrogram, the intensity profiles of the lines in function of the wavelength or of the distance from the shock may be deduced. They may also be compared to computed spectra (Fig.24) and the evolution of rotational and vibrational temperatures (or vibrational populations) may be determined: thus, in Fig.25, such an evolution is presented for a CO_2/N_2 mixture and compared to a simulated evolution.

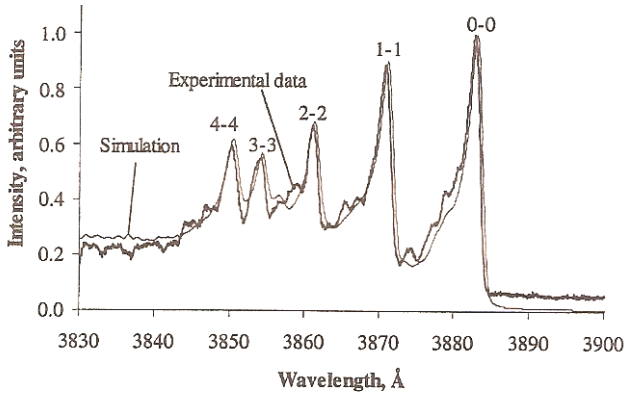

Figure 24: Experimental and calculated spectra of *CN* in $N_2/CH_4/Ar$

(Conditions of Fig.23)

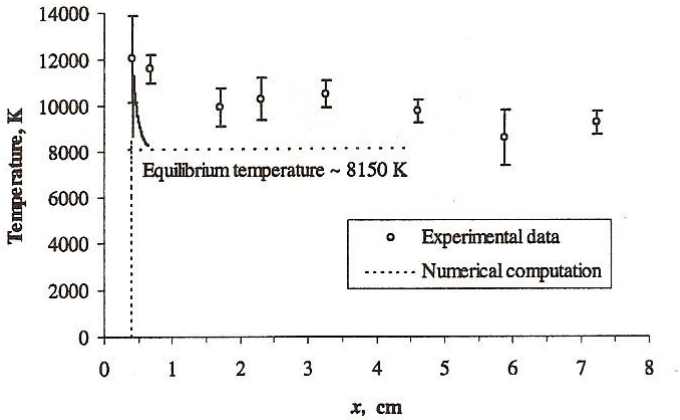

Figure 25: Evolution of vibrational temperature behind a shock in CO_2/N_2 mixture

(U_s =5800m/s, p_1 =196Pa)

REFERENCE

[1] A.G.Gaydon, I.R.Hurle, *The Shock Tube in High Temperature Chemical Research*, Chapman and Hall, London (1963)

[2] A.Ferri (Ed), *Fundamental Data Obtained from Shock Tube Experiments*, Pergamon Press (1961)

[3] G.N.Bradley, *Shock Waves in Chemistry and Physics*, London (1962)

[4] H.Oertel, *Stossrohre*, Springer-Verlag, Wien (1966)

[5] Y.V.Stupochenko, S.A.Losev, A.I.Osipov, *Relaxation in Shock Waves*, Springer-Verlag, Berlin (1967)

[6] L.Z.Dumitrescu, *Cercetari in Tuburile de Soc*, Ed. Acad. Rep. Soc. Rom. Bucuresti (1969)

[7] H.Mirels, *Phys. Fluids*, 6, 1201 (1963)

[8] J.Sidès, R.Brun, *J. Mec.*, 14, 3, 387 (1975)

[9] D.Zeitoun, M.Imbert, *AIAA J.*, 17, 8, 821 (1979)

[10] H.Mirels, *AIAA J.*,2, 1, 84 (1964)

[11] C.J.Doolan, P.A.Jacobs, *AIAA J.*, 34, 6, 1291 (1996)

[12] D.R.White, *J. Fl. Mech.*, 4, 585 (1958)

[13] C.J.S.Simpson, T.R.Chandler, K.B.Bridgman, *Phys. Fluids*, 10, 1894 (1967)

[14] R.S.Hickman, L.C.Farrar, J.B.Kyser, *Phys. Fluids*, 18, 1249 (1970)

[15] R.Brun, R.Reboh, *AIAA J.*, 15, 9, 1344 (1977)

[16] D.Zeitoun, R.Brun, M.J.Valetta, *Shock Tubes and Waves*, 180, The Magness Press, Jerusalem (1980)

[17] K.Tajima, E.Outa, G.Nakada, *Bull. JSME*, 11, 43 (1968)

[18] A.Hartunian, A.L.Russo, P.V.Marrone, *J. Aerosp. Sci.*, 27, 8, 587 (1960)

[19] R.Brun, P.Auberger, N.G. Van Que, *Acta Astronautica*, 5, 1145 (1978)

[20] A.Herzberg, W.E.Smith, M.S.Glick, W.Squire, *Cornell Aero. Lab. Rep.* AD-789 A.2 (1955)

[21] H.Mark, *J. Aero. Sci.*, 24, 304 (1957)

[22] M.P.Dumitrescu, *Shock Waves*, 1581, World Scientific, Singapore (1995)

[23] A.J.Neely, R.G.Morgan, *Aeronaut. J.*, 946, 175 (1994)

[24] H.R.Yu, B.Esser, M.Lennartz, H.Grönig, *Shock Waves*, 245, Springer-Verlag, Berlin, (1992)

[25] R.J.Stalker, *AIAA J.*, 5, 12, 2160 (1967)

[26] H.Hornung, *GALCIT Rep.* FM 88-1 (1988)

[27] M.P.Dumitrescu, *Shock Waves*, 1487, World Scientific, Singapore (1995)

[28] K.Itoh, *Shock Waves*, 43, World Scientific, Singapore (1995)

[29] Y.Burtschell, R.Brun, D.Zeitoun, *Shock Waves*, 583, Springer-Verlag, Berlin (1992)

[30] C.Chartier, R.Brun, Y.M.Grellier, *Les tubes à choc: Conception et recherches*, Pub. Sci Tech. Ministère de l'Air, N.T. 130 (1963)

[31] N.Belouaggadia, T.Hashimoto, S.Nonaka, K.Takayama, R.Brun, *AIAA J.*, 45, 6, 1420 (2007)

[32] A.Chaix, M.P.Dumitrescu, L.Z.Dumitrescu, R.Brun, *Shock Waves, 21st ISSW*, Paper 2061, Great Keppel (1997)

[33] R.N.Schwartz, Z.I.Slavsky, K.F.Herzfeld, *J. Chem. Phys.*, 20, 1591 (1952)

[34] R.C.Millikan, D.R.White, *J. Chem. Phys.*, 39, 3209 (1963)

[35] J.P.Martin, M.R.Buckingham, J.A.Chenery, C.J.S.M. Simpson, *J. Chem. Phys.*, 74, 15 (1983)

[36] J.G.Meolans, R.Brun, *Rarefied Gas Dynamics*, 345, Teubner, Stuttgart (1986)

[37] I.R.Hurle, A.L.Russo, J.G.Hall, *J. Chem. Phys.*, 40, 2076 (1964)

[38] S.Sharma, S.M.Ruffin, W.D.Gillespie, S.A.Meyer, *J. Therm. Heat Transf.*, 7, 4, 697 (1993)

[39] H.Pilverdier, R.Brun, M.P.Dumitrescu, *J. Therm. Heat Transf.*, 15, 4, (2001)

[40] D.Ramjaun, M.P.Dumitrescu, R.Brun, *J. Therm. Heat Transf.*, 13, 2, 219 (1999)